Anomalous Difference in Magnetic Behavior between Highly Saddled Iron(III) Porphyrin Complexes in the Solid State

Yoshiki Ohgo,*[a] Takahisa Ikeue,[a] Masashi Takahashi,[b] Masuo Takeda,[b] and Mikio Nakamura*[a,c]

Dedicated to the late Professor Oyo Mitsunobu of Aoyama Gakuin University

Keywords: Iron / Porphyrinoids / Spin crossover / Magnetic properties

The spin states of microcrystalline samples of $[Fe(OMTPP)L_2]^+$ (L = DMAP or Py) have been examined and interpreted using Mössbauer spectroscopy, SQUID magnetometry and X-ray crystallography. The Mössbauer spectra of $[Fe(OMTPP)(DMAP)_2]^+$ and $[Fe(OMTPP)Py_2]^+$ showed that both of these complexes maintain the low-spin (S = 1/2) state over the 77–300 K temperature range. The spin states of these complexes were further confirmed by SQUID magnetometry. Thus, the magnetic behavior of $[Fe(OMTPP)Py_2]^+$ is quite different from that of the structurally related species $[Fe(OETPP)Py_2]^+$. The latter complex exhibits a novel spin crossover between the S = 3/2 and S = 1/2 states as revealed by the spectroscopic and magnetic measurements. In order to understand the reasons for the absence of the spin crossover process in $[Fe(OMTPP)Py_2]^+$, we have compared the crystal and molecular structures of $[Fe(OMTPP)Py_2]^+$ with those of the recently reported species $[Fe(OETPP)Py_2]^+$. In the case of $[Fe(OMTPP)Py_2]^+$, the Fe–N_{axial} bond lengths hardly change with temperature and are 2.058(6) and 2.024(4) Å at 298 and 80 K, respectively. These results are in sharp contrast to those of the spin crossover complex $[Fe(OETPP)Py_2]^+$, in which the Fe–N_{axial} bonds contract from 2.201(3) Å at 298 K to 1.993(3) Å at 80 K. We have ascribed the difference in magnetic behavior between $[Fe(OMTPP)Py_2]^+$ and $[Fe(OETPP)Py_2]^+$ to the difference in molecular packing; the former adopts a densely packed cubic crystal system while the latter shows a less condensed monoclinic system. A cavity calculation has further confirmed the above mentioned assumption. While the cavity sizes around the pyridine ligands in $[Fe(OETPP)Py_2]^+$ are 32.08 and 28.88 $Å^3$ at 298 K, that in $[Fe(OMTPP)Py_2]^+$ is only 19.81 $Å^3$. Furthermore, the cavities contract by 17.7% in $[Fe(OETPP)Py_2]^+$ when the temperature is lowered from 298 to 80 K whereas the contraction is only 5.3% in the case of $[Fe(OMTPP)Py_2]^+$. On the basis of these results, we have concluded that the loosely packed crystal system and the wide cavities around the axial ligands are the important requirements for the occurrence of the spin crossover process in the solid state.

Introduction

The spin states of iron(III) porphyrin complexes are controlled by several factors[1−3] the most important being the number and nature of the axial ligands. For example, axially bound strong field ligands such as cyanide, imidazole, and pyridine form low-spin (S = 1/2) six-coordinate complexes. In contrast, anionic ligands such as Cl^- and F^- lead to the formation of five-coordinate high-spin (S = 5/2) complexes. Maltempo discussed a quantum mechanically spin admixed S = 3/2, 5/2 state and suggested that the S = 3/2 state is an important contributor to the spin states of cytochromes c′, which are recognized as histidine ligated five-coordinate iron(III) complexes.[4−6] In fact, the mono(imidazole) complexes of iron(III) porphyrin exhibit the S = 3/2, 5/2 admixed intermediate-spin in a series of $[Fe(TMP)(R-Im)]^+$ complexes, where R−Im indicates alkyl-substituted imidazoles and benzimidazoles.[7−9] In general, the degree of the S = 3/2 contribution in five-coordinate complexes correlates with the ligand field of the anionic axial ligands - it increases as the ligand field of the axial ligands weakens. Reed and co-workers thus ranked the relative field strengths of weak anionic ligands (X) in [Fe(TPP)X] on the basis of spectroscopic and magnetic properties and called the resultant hierarchy a magnetochemical series.[10,11] We and others have recently reported that the deformation of the porphyrin ring is also an important factor which affects the spin states[12,13] and the electron configurations of iron(III) ions.[14−21] Thus, highly nonplanar six-coordinate com-

[a] Department of Chemistry, School of Medicine, Toho University,
Tokyo 143-8540, Japan
Fax: (internat.) + 813-5493-5430
E-mail: mnakamu@med.toho-u.ac.jp (M. N.)
yohgo@med.toho-u.ac.jp (Y. O.)
[b] Department of Chemistry, Faculty of Science, Toho University, Funabashi 274-8510, Japan
[c] Division of Biomolecular Science, Graduate School of Science, Toho University,
Funabashi 274-8510, Japan

  DOI: 10.1002/ejic.200300566

plexes with weak field axial ligands such as the saddled $[Fe(OETPP)(THF)_2]^+$ and the ruffled $[Fe(T\textit{i}PrP)(THF)_2]^+$ exhibit an essentially pure intermediate spin state.[12] These results have been ascribed to the short $Fe-N_p$ (N_p: nitrogen atoms of porphyrin) bond lengths caused by the nonplanarity of the porphyrin rings[12,13,22–25] together with the weak coordinating ability of the axial ligands.[10,11] The strongly S_4 saddled OETPP ring stabilizes the intermediate spin state even in the presence of nitrogen bases. Thus the complexes $[Fe(OETPP)L_2]^+$ (L = Py and 4-CNPy) show the $S = 3/2$ state at room temperature and exhibit a novel spin transition from the $S = 3/2$ to the $S = 1/2$ state as the temperature is lowered.[26] In this paper, we report on the spin states of other saddle shaped complexes, namely $[Fe(OMTPP)L_2]^+$ (L = DMAP and Py) in the solid state on the basis of a combined analysis by Mössbauer spectroscopy, SQUID magnetometry, and X-ray crystallography. We also report on the anomalous difference in magnetic behavior between the structurally similar $[Fe(OMTPP)Py_2]^+$ and $[Fe(OETPP)Py_2]^+$ in the solid state and on the requirements for the occurrence of the spin crossover process (Scheme 1).

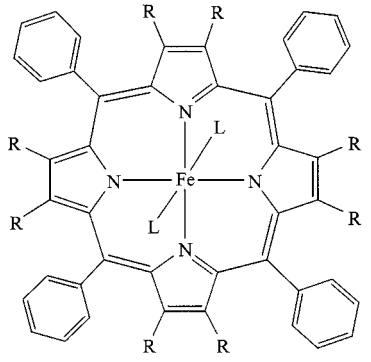

$[Fe(OMTPP)L_2]^+$ (R = Methyl)
$[Fe(OETPP)L_2]^+$ (R = Ethyl)
L = DMAP, Py

Scheme 1

Results and Discussion

Structural Characteristics

Figure 1 shows the molecular structure of $[Fe(OMTPP)(DMAP)_2]ClO_4 \cdot 4CHCl_3$ determined at 298 K. Two of the four solvent molecules and a counter anion (not shown) exhibit two disordered structures, A and B, in each site. The site-occupancy factors of the two solvent molecules and the counter anion for A:B are 0.85:0.15, 0.72:0.28, and 0.54:0.46, respectively. Figure 2 shows the molecular structure of $[Fe(OMTPP)Py_2]ClO_4 \cdot 1/3HClO_4 \cdot 4/3CHCl_3$ determined at 298 K. Because the Fe1, N2, and C16 atoms lie on the four-fold inverted axis, only a quarter of the molecule is crystallographically independent. Similarly, because Cl1, O2, C17, and H17 are on the three-fold axis, one-third of the counter anion and solvent molecules are in an asymmetric unit. The counter anion is disordered and the site-occupancy factors for the disordered O1A and O1B are 0.59 and 0.41, respectively, at 298 K. The structure of the counter anion at 80 K is, however, ordered as a consequence of the increase in the packing force and the decrease in the thermal movement of the molecule. Figure 3 shows the molecular structure of $[Fe(OETPP)(DMAP)_2]ClO_4$ determined at 298 K. This crystal turns out to be a polymorph of the crystal reported previously by Walker et al.[27] The present crystal, the polymorph A, with the space group $P3_121$ (#152) contains no solvent molecules, while the crystal reported by Walker et al., the polymorph B, with space group $Pna2_1$ (#33) contains four chloroform molecules in crystallographically independent space. Figure 4 shows the deviation of each atom in $[Fe(OMTPP)L_2]^+$ (L =

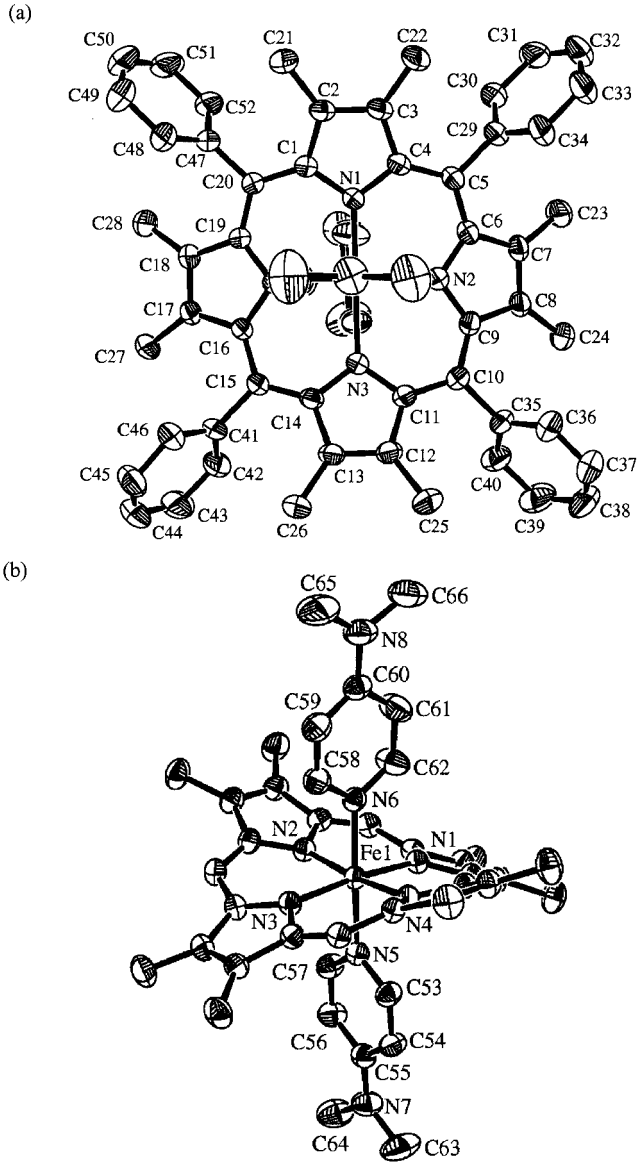

Figure 1. ORTEP diagrams of $[Fe(OMTPP)(DMAP)_2]^+$ together with the atom labeling; thermal ellipsoids are drawn at the 50% probability level: (a) top view (b) side view; phenyl rings are omitted for clarity in (b)

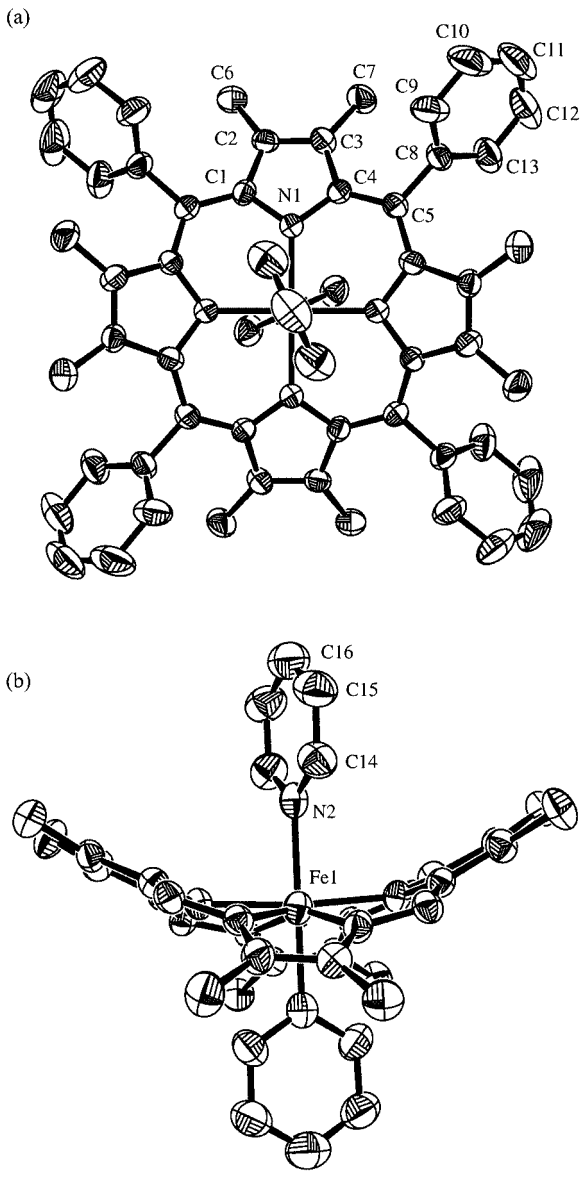

Figure 2. ORTEP diagrams of $[Fe(OMTPP)Py_2]^+$ together with the atom labeling for the unique quarter of the porphyrin; thermal ellipsoids are drawn at the 50% probability level: (a) top view (b) side view; phenyl rings are omitted for clarity in (b)

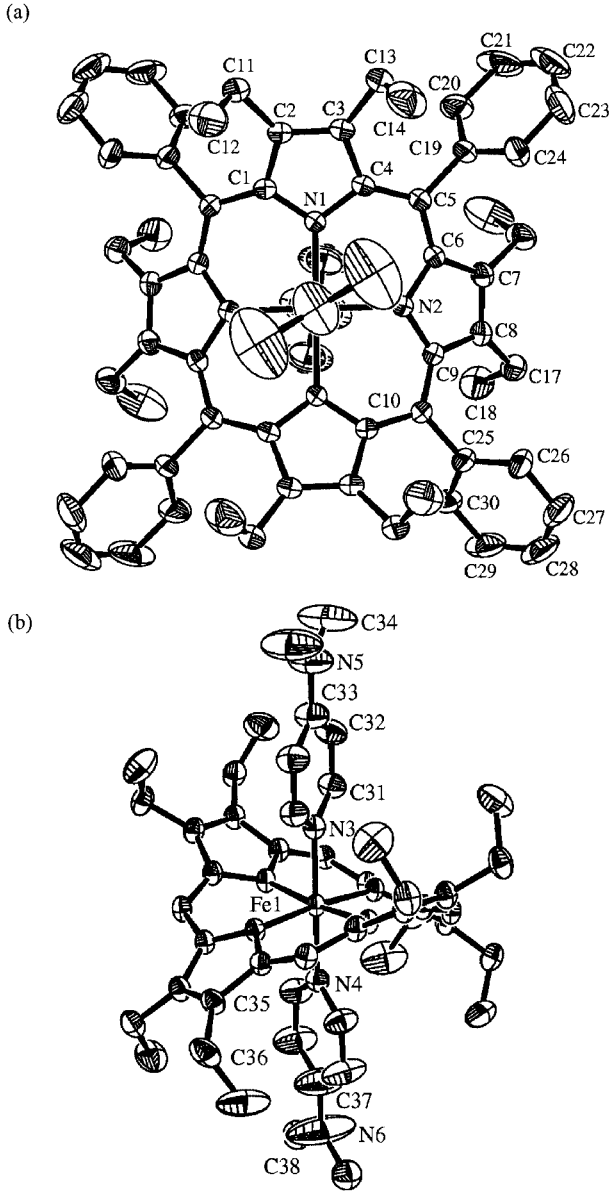

Figure 3. ORTEP diagrams of $[Fe(OETPP)(DMAP)_2]^+$ together with the atom labeling for the unique quarter of the porphyrin; thermal ellipsoids are drawn at the 50% probability level: (a) top view (b) side view; phenyl rings are omitted for clarity in (b)

DMAP, Py) and $[Fe(OETPP)L_2]^+$ (L = DMAP, Py[28]) from the average plane defined by the 24-atom porphyrin cores. Table 1 lists the crystal data for $[Fe(OMTPP)L_2]ClO_4$ (L = DMAP and Py) and $[Fe(OETPP)L_2]ClO_4$ (L = DMAP and Py[28]). Table 2 lists some structural parameters of the complexes[27,28] which are defined as follows: φ is the orientation angle of the axial ligand to the nearest N_P-Fe-N_P axis, θ is the dihedral angle between two axial ligands, τ is the dihedral angle between the average N4 plane and each pyrrole ring, ψ is the dihedral angle between two diagonal pyrrole rings, η is the twist angle between two diagonal pyrrole rings, ω is the dihedral angle between the phenyl group and the $C_\alpha-C_{meso}-C_{\alpha'}$ plane, and $|\Delta C_{meso}|$ and $|\Delta C_\beta|$ are the deviations of the *meso* and β-pyrrole carbon atoms from the mean porphyrin plane, respectively. They are also given in Scheme 2.

Figure 1 and Figure 4(a) clearly show that the porphyrin core of $[Fe(OMTPP)(DMAP)_2]^+$ is highly saddled. The average $Fe-N_p$ bond length of 1.979(3)Å is slightly shorter than that of 1.989 Å in the typical low-spin complex, $[Fe(TPP)(1\text{-}MeIm)_2]^+$.[29] The average $Fe-N_{axial}$ bond length of 2.009 Å is also quite close to the corresponding bond lengths of low-spin $[Fe(TPP)Py_2]^+$ and $[Fe(OEP)(DMAP)_2]^+$ which are 2.003 and 1.995 Å, respectively.[30,31] The β-pyrrole carbon atoms of each pyrrole ring are alternately displaced, on average, by ±0.94 Å from the 24-atom mean porphyrin plane. Because of the highly saddled structure, the complex has two mutually perpendicular clefts along the diagonal N_p-Fe-N_p axes. The DMAP ligands are situated almost exactly along these clefts. Thus, the φ values are only 1.3(3)° and 2.4(4)°. The

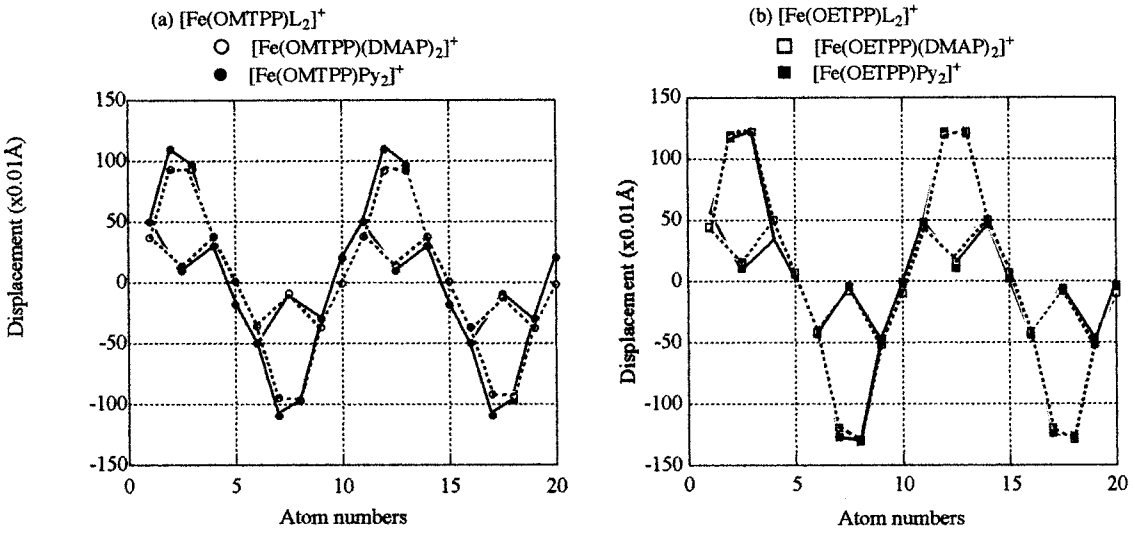

Figure 4. Perpendicular displacement of the peripheral carbon and nitrogen atoms of (a) $[Fe(OMTPP)L_2]^+$ and (b) $[Fe(OETPP)L_2]^+$ in units of 0.01 A, where L = DMAP and Py

Table 1. Crystal data of OMTPP and OETPP complexes

	$[Fe(OMTPP)(DMAP)_2]ClO_4$	$[Fe(OMTPP)(Py)_2]ClO_4$	$[Fe(OMTPP)(Py)_2]ClO_4$	$[Fe(OETPP)(DMAP)_2]ClO_4$
T(K)	298	298	80	298
Chemical Formula	$C_{66}H_{64}N_8O_4FeCl \cdot (CHCl_3)_4$	$C_{62}H_{54}N_6O_4FeCl \cdot (H_{0.33}Cl_{0.33}O_{1.33})$ $(C_{1.33}H_{1.33}Cl_4)$	$C_{62}H_{54}N_6O_4FeCl \cdot (H_{0.33}Cl_{0.33}O_{1.33})$ $(C_{1.33}H_{1.33}Cl_4)$	$C_{74}H_{80}N_8FeCl$
Crystal dimension(mm)	0.2 x 0.1 x 0.1	0.5 x 0.5 x 0.3	0.1 x 0.1 x 0.1	0.5 x 0.4 x 0.1
Crystal color	purple	purple	purple	purple
Crystal system	Monoclinic	Cubic	Cubic	Trigonal
Space group	$P2_1/c$ (#14)	I43d (#220)	I43d (#220)	$I3_121$(#152)
Mr	1602.02	1230.72	1230.72	1172.76
a (Å)	16.4556(5)	25.937(3)	25.609(1)	22.595(9)
b (Å)	23.7289(6)	25.937(3)	25.609(1)	22.595(9)
c (Å)	19.8424(6)	25.937(3)	25.609(1)	13.967(5)
α (°)	90	90	90	90
β (°)	91.924(1)	90	90	90
γ (°)	90	90	90	120
V (Å^3)	7743.6(4)	17448(3)	16795.5(9)	6175(4)
Z	4	12	12	3
Dx (Mg m^{-3})	1.374	1.406	1.460	0.946
Diffractometer	Rigaku RAXIS-RAPID Imaging Plate	Rigaku AFC-7R	Rigaku RAXIS-RAPID Imaging Plate	Rigaku RAXIS-RAPID Imaging Plate
Scan type	ω-scan	ω-scan	ω-scan	ω-scan
Absorption correction	multi-scan (T_{min} =0.869, T_{max} = 0.933)	ψ-scan (T_{min} =0.763, T_{max} = 0.845)	none	multi-scan (T_{min} =0.885, T_{max} = 0.975)
$2\theta_{max}$ (°)	55.0 (-19 < h < 21, -30<k<30, -25<l<25)	55.0 (-18 < h < 33, 0<k<23, -10<l<19)	55.0 (-33 < h < 33, -23<k<23, -17<l<18)	55.0 (-29 < h < 29, -29<k<29, -18<l<18)
No. of Indep. reflns.	17126	1948	3090	9164
No. of reflns with > 2σ(I)	11710	1290	2512	8884
No. of parameters	935	204	196	413
R_{int}	0.0546	0.0362	0.0960	0.0615
R1	0.0889	0.0423	0.0536	0.0594
wR^2	0.2543	0.1143	0.1144	0.1585
S	1.024	0.989	0.961	1.087
Weighting scheme	w=1/[σ^2(Fo^2) + (0.01785P)^2+2.5869P] where P = (Fo^2 +2Fc^2)/3	w=1/[σ^2(Fo^2) + (0.0623P)^2] where P = (Fo^2 +2Fc^2)/3	w=1/[σ^2(Fo^2) + (0.0623P)^2] where P = (Fo^2 +2Fc^2)/3	w=1/[σ^2(Fo^2) + (0.1236P)^2+0.4276P] where P = (Fo^2 +2Fc^2)/3
$(\Delta/\sigma)_{max}$	<0.001	<0.001	<0.001	<0.001
$\Delta\rho_{max}$ (eÅ^{-3})	0.906	0.192	0.819	0.991
$\Delta\rho_{min}$ (eÅ^{-3})	-0.725	-0.248	-0.527	-0.300

dihedral angle θ between the two DMAP ligands is 84.2°. The porphyrin core is ideally saddle shaped as indicated by the fairly small $|\Delta C_{meso}|$ and η values which are 0.01 Å and 1.3(4)°, respectively.

Replacement of the axially coordinated DMAP ligand by Py in $[Fe(OMTPP)L_2]^+$ causes some structural changes as shown in Figure 2 and Figure 4(a). The largest change is the elongation of the Fe−N_{axial} bonds from 2.009(3) to

Table 2. Comparison of structural parameters $[Fe(OMTPP)L_2]^+$ and $[Fe(OETPP)L_2]^+$

Complexes	T/K	Fe-N_p /Å	Fe-N_{axial} /Å	ϕ / °	θ / °	τ / °	ψ / °	η / °	ω / °	$\lvert\Delta C_{meso}\rvert$ / 0.01Å	$\lvert\Delta C_\beta\rvert$ / 0.01Å	Cavity /Å^3	Ref
$[Fe(OMTPP)(DMAP)_2]^+$	298	1.979(3)	2.009	1.3(3) 2.4(4)	84.2	22.3(2)	143.0(2)	1.3(4)	56.0(2)	1	94	——	this work
$[Fe(OMTPP)Py_2]^+$	298	1.963(3)	2.058(6)	24.8(3)	90	26.1(1)	128.2(1)	10.0(3)	45.2(1)	19	104	19.81	this work
$[Fe(OMTPP)Py_2]^+$	80	1.973(3)	2.024(4)	23.4(2)	90	25.9(1)	128.5(1)	10.2(3)	45.4(1)	18	102	18.77	this work
$[Fe(OETPP)(DMAP)_2]^+$	298	1.977(2)	2.030(3)	10.6(2) 25.0(2)	53.2	30.8(1)	118.4(1)	4.0(2)	66.7(2)	8	122	——	this work
$[Fe(OETPP)(DMAP)_2]^+$	298	1.951	2.000	9 29	70	33[a]	114[a]	17[a]	66	28	122	——	[27]
$[Fe(OETPP)Py_2]^+$	298	1.985	2.201	1.1(4) 3.6(3)	82.3	32.4(1)[b]	115.2(2)[b]	1.2(3)[b]	40.6(1)	3	124	28.88 32.08	[28]
$[Fe(OETPP)Py_2]^+$	80	1.957	1.993	6.3(3) 11.6(3)	85.1	30.8(1)[b]	118.5(1)[b]	3.0(3)[b]	64.5(3)	6	121	23.19	[28]

[a] The angles are calculated on the basis of the molecular structure reported by Ogura et al.[27] [b] The angles are calculated on the basis of the molecular structure reported in our previous paper.

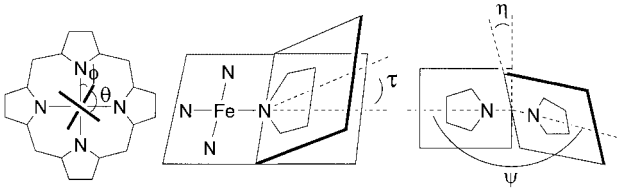

Scheme 2

2.058(6) Å. In contrast, the Fe−N_p bonds exhibit a small contraction of 0.016 Å. These results can be explained in terms of the difference in ligand field strength between DMAP and Py since DMAP is a much stronger field ligand than Py. Thus, the replacement of DMAP by Py weakens the axial coordination and lengthens the Fe−N_{axial} bonds, which in turn strengthens the equatorial coordination and causes concomitant contraction of the Fe−N_p bonds. The saddled motif in $[Fe(OMTPP)Py_2]^+$ is much deeper than that in $[Fe(OMTPP)(DMAP)_2]^+$ as indicated by the increase in the $|\Delta C_\beta|$ and τ values and the decrease in the ψ value; $|\Delta C_\beta|$ increases from 0.94 to 1.04 Å while ψ decreases from 143.0 to 128.2°. The $|\Delta C_{meso}|$ and η values are also different for two complexes - they are 0.01 Å and 1.3(4) ° for the DMAP, and 0.19 Å and 10.0(3)° for the Py complex. Such results indicate that, in contrast to the case of $[Fe(OMTPP)(DMAP)_2]^+$, the saddled structure of $[Fe(OMTPP)Py_2]^+$ contains some ruffling. Due to the mixing of the ruffled deformation, the mutually perpendicular clefts which are located along the diagonal N_p−Fe−N_p axes in the DMAP complex rotate to some extent about the Fe−N_{axial} axis. As a result, the axial ligands are aligned along the new clefts. This must be the reason why the φ value increased to 24.8(3)°.

As mentioned, $[Fe(OETPP)(DMAP)_2]^+$ has two polymorphs, A and B. Structural parameters of the polymorph A such as τ, ψ, and η are listed in Table 2. The same parameters of the polymorph B have been calculated on the basis of the molecular structure reported by Walker and co-workers[27] and these are also listed in Table 2. The average Fe−N_p and Fe−N_{axial} bond lengths are 1.977(2) and 2.030(3)Å in polymorph A, while those in polymorph B are 1.951Å and 2.000Å, respectively. The $|\Delta C_{meso}|$ and η values in A and B are also different from each other - they are 0.08 Å and 4.0° in A, and 0.28 Å and 17° in B. These data indicate that the saddled porphyrin ring in polymorph B contains some ruffling. The dihedral angles θ in A and B are 53.2° and 70°, respectively, which are much smaller than those of the other complexes.

The structural parameters of $[Fe(OMTPP)(DMAP)_2]^+$ can now be compared with those of polymorph A of $[Fe(OETPP)(DMAP)_2]^+$. As shown in Figure 3 and Figure 4(b), the saddled structure has increased on going from the OMTPP to the OETPP complex. The $|\Delta C_\beta|$ and ψ values are 0.94 Å and 143.0(2)° in $[Fe(OMTPP)(DMAP)_2]^+$ while they are 1.22 Å and 118.4(1)° in $[Fe(OETPP)(DMAP)_2]^+$. Although the average Fe−N_{axial} bond length has increased by 0.021 Å on going from OMTPP to OETPP, the average Fe−N_p bond lengths remain almost constant. In contrast to the ideally saddle shaped $[Fe(OMTPP)(DMAP)_2]^+$, the porphyrin core of $[Fe(OETPP)(DMAP)_2]^+$ exhibits a slight ruffling as revealed by the larger $|\Delta C_{meso}|$ and η values of 0.08 Å and 4.0(2)°. As a result, the φ values of the axial ligands have increased from 1.3(3)° and 2.4(4)° in $[Fe(OMTPP)(DMAP)_2]^+$ to 10.6(2) and 25.0(2)° in $[Fe(OETPP)(DMAP)_2]^+$.

Similarly, the structural parameters of $[Fe(OMTPP)Py_2]^+$ can be compared with those of $[Fe(OETPP)Py_2]^+$ reported in our previous communication.[28] The largest difference can be seen in the long Fe−N_{axial} bond lengths of 2.201Å in $[Fe(OETPP)Py_2]^+$. Even the Fe−N_p bonds show a small increase of 0.022 Å. As in the case of the DMAP complexes, the saddled structure has increased on going from the

OMTPP to the OETPP complex. The $|\Delta C_\beta|$ and ψ values in $[Fe(OMTPP)Py_2]^+$ are 1.04 Å and 128.2(1)° compared with 1.24 Å and 115.2(2)° in $[Fe(OETPP)Py_2]^+$. While the porphyrin core of $[Fe(OMTPP)Py_2]^+$ exhibits some ruffling, that of $[Fe(OETPP)Py_2]^+$ shows quite a pure saddled structure. The $|\Delta C_{meso}|$ and η values are 0.03 Å and 1.2(3)°, respectively.[28] These results indicate that $[Fe(OETPP)Py_2]^+$ has two deep clefts along the diagonal N_p-Fe-N_p axes above and below the porphyrin ring. As a result, the pyridine ligands are situated almost exactly along the diagonal N_p-Fe-N_p axes and the φ values are only 1.1(4)° and 3.6(3)°. Thus, the orientation of planar axial ligands in highly saddled porphyrin complexes can be summarized as follows: the axial ligands are orientated along the diagonal N_p-Fe-N_p axes but they rotate toward the diagonal $C_{meso}-Fe-C_{meso}$ axes as the ruffling character increases.[32–34]

Table 3. Mössbauer parameters of $[Fe(OMTPP)L_2]^+$ and $[Fe(OETPP)L_2]^+$ (L = DMAP, Py)

L	T / K	IS / mm s^{-1}	QS / mm s^{-1}	Γ_1 / mm s^{-1}	Γ_2 / mm s^{-1}	Ref
OMTPP						
DMAP	290	0.16	1.86	0.30	0.33	this work
	70	0.23	1.89	0.38	0.54	
Py	299	0.19	2.18	0.23	0.26	this work
	78	0.25	2.18	0.33	0.42	
OETPP						
DMAP	290	0.19	2.21	0.27	0.32	[26]
	80	0.26	2.31	0.55	0.89	
Py	290	0.32	2.76	0.27	0.29	[26]
	70	0.25	2.29	0.47	0.64	

Spin States of $[Fe(OMTPP)L_2]^+$

(i) Mössbauer Spectra

Figure 5 shows the temperature dependence of the Mössbauer parameters such as isomer shift (IS) and quadrupole splitting (QS) for $[Fe(OMTPP)L_2]^+$ and $[Fe(OETPP)L_2]^+$ (L = DMAP, Py) determined for microcrystalline samples.[26] Table 3 lists the IS, QS and effective line widths (Γ_1 and Γ_2). The IS value increases from 0.16 to 0.23 mm·s^{-1} in the case of $[Fe(OMTPP)(DMAP)_2]^+$ as the temperature is lowered from 290 to 77 K. A similar increase has been observed for the IS values of $[Fe(OMTPP)Py_2]^+$ and $[Fe(OETPP)(DMAP)_2]^+$ which increase from 0.19 to 0.25 mm·s^{-1} and from 0.19 to 0.26 mm·s^{-1}, respectively. Only the IS value of $[Fe(OETPP)Py_2]^+$ shows a large decrease from 0.32 to 0.25 mm·s^{-1} as shown in Figure 5(a). The QS values of $[Fe(OMTPP)(DMAP)_2]^+$, $[Fe(OMTPP)Py_2]^+$, and $[Fe(OETPP)(DMAP)_2]^+$ are almost constant in the temperature range 290–77 K and are 1.86–1.90 mm·s^{-1} for $[Fe(OMTPP)(DMAP)_2]^+$, 2.13–2.18 mm·s^{-1} for $[Fe(OMTPP)Py_2]^+$, and 2.21–2.31 mm·s^{-1} for $[Fe(OETPP)(DMAP)_2]^+$. These three complexes thus maintain their low-spin states in the temperature ranges examined. The QS values of the low-spin complexes are in the range of 1.3–2.4 mm·s^{-1}.[26,35–37] In contrast, the QS value of 2.76 mm·s^{-1} for $[Fe(OETPP)Py_2]^+$ at 290 K is rather large and decreases to 2.29 mm·s^{-1} at 77 K. Since the S = 3/2 complexes are characterized by the large QS values,[10,12,13,24,26,38,39] this Mössbauer result suggests that $[Fe(OETPP)Py_2]^+$ exhibits a spin crossover from the predominantly S = 3/2 state at 290 K to the predominantly S = 1/2 state at 77 K.

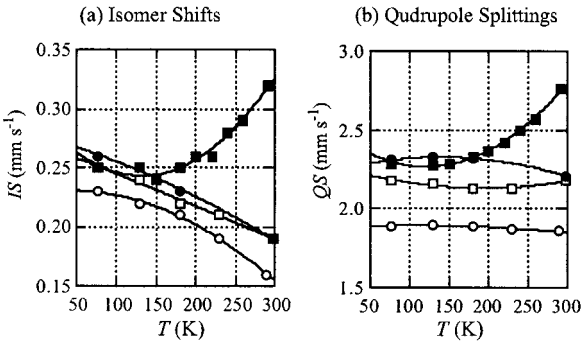

Figure 5. Temperature dependence of the Mössbauer parameters of $[Fe(OMTPP)L_2]ClO_4$ and $[Fe(OETPP)L_2]ClO_4$ measured on microcrystalline samples; open circles: $[Fe(OMTPP)(DMAP)_2]ClO_4$; open squares: $[Fe(OMTPP)Py_2]ClO_4$; filled circles: $[Fe(OETPP)(DMAP)_2]ClO_4$; filled squares: $[Fe(OETPP)Py_2]ClO_4$

(ii) SQUID Magnetometry

Figure 6 shows the temperature dependence of the effective magnetic moments of $[Fe(OMTPP)L_2]ClO_4$ (L = DMAP, Py) taken on microcrystalline samples using SQUID magnetometry. For comparison, the corresponding data for $[Fe(OETPP)L_2]ClO_4$ (L = DMAP, Py) reported in our previous communication are also given.[26] While the effective magnetic moments of $[Fe(OMTPP)(DMAP)_2]^+$, $[Fe(OMTPP)Py_2]^+$, and $[Fe(OETPP)(DMAP)_2]^+$ are 2.1–2.8 μ_B in the temperature range of 50–300 K, those of $[Fe(OETPP)Py_2]^+$ are 2.4–3.4 μ_B in the same temperature range. These results suggest that the former three complexes adopt mainly the S = 1/2 spin state while $[Fe(OETPP)Py_2]^+$ exhibits the spin transition from the predominantly S = 3/2 state to the predominantly S = 1/2 state as the temperature is lowered. The SQUID results are therefore consistent with the Mössbauer results.

Reasons for the Absence of the Spin Crossover Process in $[Fe(OMTPP)Py_2]^+$

In our previous communication, we reported the basis of the spectroscopic and magnetic results that are observed when a novel spin transition takes place from the S = 3/2 to the S = 1/2 spin state in $[Fe(OETPP)Py_2]^+$ both in solution and in the solid state as the temperature is lowered.[26] The X-ray crystallographic analysis of the same complex at three different temperatures revealed that the contraction of

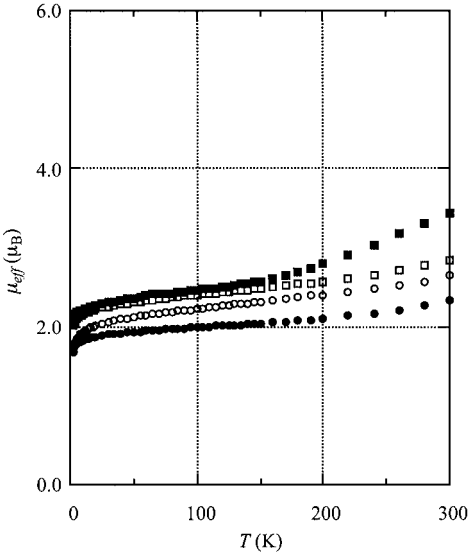

Figure 6. Temperature dependence of the effective magnetic moments of $[Fe(OMTPP)L_2]^+$ and $[Fe(OETPP)L_2]^+$ measured on microcrystalline samples using SQUID magnetometry; open circles: $[Fe(OMTPP)(DMAP)_2]ClO_4$; open squares: $[Fe(OMTPP)Py_2]ClO_4$; filled circles: $[Fe(OETPP)(DMAP)_2]ClO_4$; filled squares: $[Fe(OETPP)Py_2]ClO_4$

the Fe−N_{axial} bond is an important requirement for the spin crossover process to occur. The average Fe−N_{axial} bond length decreases from 2.201(3) to 1.993(3) Å as the temperature is lowered from 298 to 80 K.[28] Similar bond contractions have been reported by Scheidt and co-workers in $[Fe(OEP)(3\text{-}ClPy)_2]^+$, which could be ascribed to the spin transition from the $S = 5/2$ to the $S = 1/2$ state.[40,41] Thus, we expected such a spin transition should also occur in $[Fe(OMTPP)Py_2]^+$. Both the Mössbauer and SQUID measurements for the microcrystalline samples indicated, however, that such a phenomenon never occurs in the solid state. $[Fe(OMTPP)Py_2]^+$ maintains the $S = 1/2$ spin state over a wide range of temperatures. To understand the reasons for the absence of the spin crossover process in $[Fe(OMTPP)Py_2]^+$, we determined the crystal and molecular structures of this complex at 80 K. The crystal data and structural parameters are listed in Table 1 and Table 2, respectively. The data in Table 2 indicate that the Fe−N_{axial} bond in $[Fe(OMTPP)Py_2]^+$ shows only a slight decrease of 0.034 Å, as the temperature is lowered from 298 to 80 K whereas the corresponding decrease reaches as much as 0.208 Å in the case of the spin crossover complex, $[Fe(OETPP)Py_2]^+$. The data in Table 2 also indicate that the structural changes are fairly small in all respects including the values of φ, θ, τ, ω, ψ, and η. For example, while the axial ligands rotate by 5.2° and 8.0° as the temperature is lowered from 298 to 80 K in $[Fe(OETPP)Py_2]^+$, they rotate by only 1.4° in $[Fe(OMTPP)Py_2]^+$. These data are consistent with the Mössbauer and SQUID results, which indicate that $[Fe(OMTPP)Py_2]^+$ maintains the $S = 1/2$ spin state over a wide range of temperatures in the solid state.

The difference in the magnetic behavior can be ascribed to the difference in molecular packing between $[Fe(OMTPP)Py_2]^+$ and $[Fe(OETPP)Py_2]^+$ in the crystal lattices. The crystal data listed in Table 1 as well as those of $[Fe(OETPP)Py_2]^+$ reported in our previous communication indicate that the crystal systems for $[Fe(OMTPP)Py_2]^+$ and $[Fe(OETPP)Py_2]^+$ are different. The former adopts a cubic while the latter exhibits a monoclinic crystal system.[28] The monoclinic system is a less condensed packing form than the cubic system since the latter is the closest packing form as shown in Figure 7 (a and b). In fact, the density (D_x) of $[Fe(OMTPP)Py_2]^+$ with the cubic crystal system is 1.406 g cm^{-3}, while that of monoclinic $[Fe(OMTPP)(DMAP)_2]^+$ is 1.374 g cm^{-3} in spite of its larger molecular weight. It should be noted that the D_x value of the spin crossover complex, $[Fe(OETPP)Py_2]^+$, is only 1.296 g cm^{-3} at 298 K. Thus, $[Fe(OMTPP)Py_2]^+$ is the most densely packed among the three complexes. In other words, the Fe−N_{axial} bond contraction in $[Fe(OMTPP)Py_2]^+$ at lower temperature must be more difficult than that in $[Fe(OETPP)Py_2]^+$ since each molecule of $[Fe(OMTPP)Py_2]^+$ is placed in a densely packed crystal lattice even at ambient temperature. Consequently the spin crossover process, which requires a decrease in the Fe−N_{axial} bond length caused by the contrac-

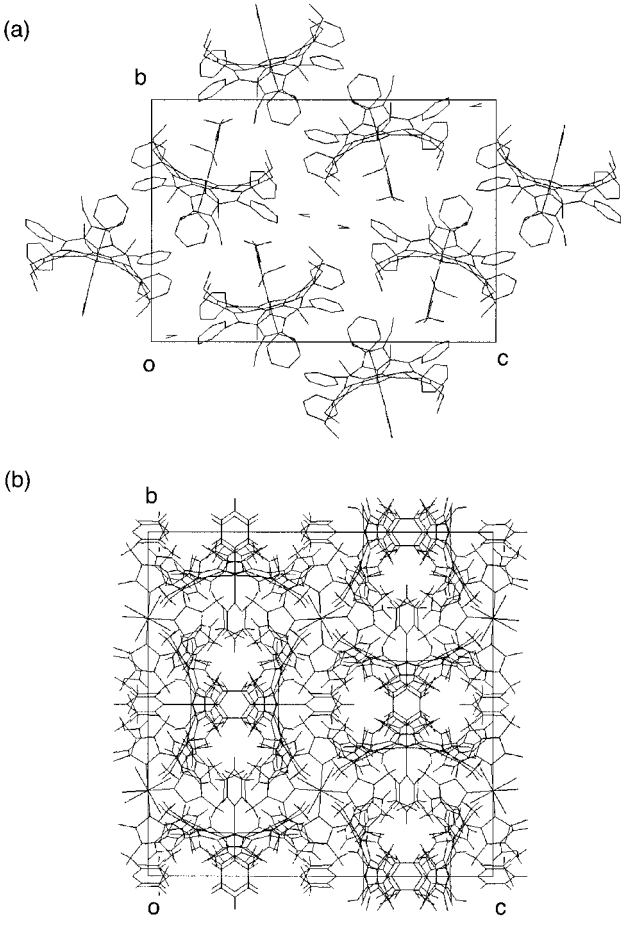

Figure 7. Crystal packing diagrams of (a) monoclinic $[Fe(OETPP)Py_2]^+$ and (b) cubic $[Fe(OMTPP)Py_2]^+$ viewed along the *a* axis

tion of the unit cell, takes place only in $[Fe(OETPP)Py_2]^+$. It should also be noted that the decrease in the crystal lattice occurs differently between $[Fe(OMTPP)Py_2]^+$ and $[Fe(OETPP)Py_2]^+$ because of the difference in crystal systems. Since the structure of $[Fe(OMTPP)Py_2]^+$ adopts a cubic system, the contraction of the crystal lattice should occur isotropically as the temperature is lowered. In the case of $[Fe(OETPP)Py_2]^+$, however, an anisotropic contraction is expected at lower temperature because of its monoclinic system. In fact, we have observed quite a direction-dependent contraction as reported in our previous communication. The major contraction takes place along the *b*-axis, which is tilted by only 15° from the $Fe-N_{axial}$ axis.[28] Thus, the contraction of the unit cell along the b-axis specifically decreases the $Fe-N_{axial}$ bonds and, consequently, induces the spin crossover process.

As mentioned, the displacement and rotation of the axial ligands are the major driving forces for the spin-crossover process in $[Fe(OETPP)Py_2]^+$.[28] The degree of displacement and rotation should correlate closely with the shape and size of the cavity around the axial ligand. The axial ligands situated in a wide cavity could easily alter their positions when the external conditions such as temperature and pressure are changed. In this respect, quantitative elucidation of the cavities around the axial ligands is quite important for clarifying the mechanism of the spin-crossover process. To reveal the spatial environment around the axial ligands of $[Fe(OETPP)Py_2]^+$ and $[Fe(OMTPP)Py_2]^+$, we have carried out a CAVITY calculation developed by Ohashi and co-workers.[42,43] In this calculation, the cavity for the axial ligand is defined as the concave space limited by the surface of the spheres,[42,43] where each atom in the vicinity of the pyridine ligand is located in the center of the sphere with the radius of each sphere being greater than the van der Waals radius by 1.2 Å.[44] Figure 8 (a and b) exhibit the change in orientation of the pyridine ligand of $[Fe(OMTPP)Py_2]^+$ as the temperature is lowered from 298 to 80 K. In this complex, a quarter of the molecule is crystallographically independent. Thus, the cavity size and shape of each ligand is exactly the same in a single molecule. Figure 8 (c and d) illustrate the change in orientation of one of the pyridine ligands of $[Fe(OETPP)Py_2]^+$. Since the complex has two independent pyridine ligands in a single molecule, the cavities of the ligands are different from each other. The cavity sizes of these complexes are also listed in Table 2. The data in Table 2 clearly indicate that the cavity sizes are quite different between the two complexes. The OETPP complex showing the spin-crossover phenomenon has cavities of 32.08 and 28.88 $Å^3$ at 298 K, while the OMTPP complex has a much smaller cavity size of 19.81$Å^3$. Thus, the cavity size of the Py ligand in $[Fe(OMTPP)Py_2]^+$ is only 65% of that in $[Fe(OETPP)Py_2]^+$. Close inspection of the cavities in Figure 8 (c and d) reveals that the pyridine ligand in the OETPP complex, signified as a bold line, is aligned along the diagonal N1−N3 axis and makes contact with a convex surface created by the neighboring atoms at 298 K. When the temperature is lowered to 80 K, the $Fe-N_{axial}$ bond contracts. Concomitantly, the pyridine ligand rotates toward the diagonal $C_{meso}-C_{meso}$ axis to minimize the repulsion with the porphyrin core until it makes contact with another convex surface. In other words, each pyridine ligand of $[Fe(OETPP)Py_2]^+$ has room for rotation, which in turn enables the contraction of the $Fe-N_{axial}$ bond and makes the spin crossover possible. In contrast, the pyridine ligand in $[Fe(OMTPP)Py_2]^+$ is confined to a limited space of only 65% of that available in $[Fe(OETPP)Py_2]^+$. Furthermore, the cavity shape around the pyridine ligand does not allow any rotation of the ligand as shown in Figure 8 (a and b). Both sides of the pyridine ligand make contact with the convex surfaces. Another notable difference is the compression ratio of the cavity as the temperature is lowered from 298 to 80 K. Although the cavity of the OETPP complex decreases on average by 17.7%, that of the OMTPP complex shows a much smaller decrease of 5.25%. Thus, the absence of the spin crossover process in $[Fe(OMTPP)Py_2]^+$ can be attributed to the fact that the molecules are placed in a densely packed crystal lattice even at room temperature and that the axial ligands are confined to narrow cavities. In other words, a loosely packed crystal system and wide cavities around the axial ligands which allow their displacement and rotation are the important requirements for the spin transition to occur in the solid state.

Conclusions

Combined analysis using Mössbauer spectroscopy and SQUID magnetometry has revealed that the spin state of the saddle shaped complex $[Fe(OMTPP)Py_2]^+$ is quite different from that of the corresponding $[Fe(OETPP)Py_2]^+$. While $[Fe(OETPP)Py_2]^+$ exhibited a novel spin crossover process over 80−300 K, $[Fe(OMTPP)Py_2]^+$ maintained the $S = 1/2$ spin state in the same temperature range. The molecular structures of $[Fe(OMTPP)Py_2]^+$ determined at 298 and 80 K by X-ray crystallography further support the Mössbauer and SQUID results. The $Fe-N_{axial}$ bond contraction, which is one of the most important requirements for the spin crossover process to occur, is only 0.034 Å even if the temperature is lowered from 298 to 80 K whereas the bond contraction reaches as much as 0.208 Å in the case of $[Fe(OETPP)Py_2]^+$. To further understand the spin crossover process in the solid state, we have determined the cavity size of each ligand in $[Fe(OMTPP)Py_2]^+$ and $[Fe(OETPP)Py_2]^+$ by Ohashi's method.[42−44] While the OETPP complex has cavities of 32.08 and 28.88 $Å^3$, the OMTPP complex exhibits a much smaller cavity with a volume of 19.81 $Å^3$. Furthermore, the cavities of the OETPP complex decreased by 15.6 and 19.7% as the temperature was lowered from 300 to 80 K. In contrast, the contraction of the cavity in the OMTPP complex was only 5.3%. On the basis of these results, we conclude that the absence of the spin crossover process in $[Fe(OMTPP)Py_2]^+$ can be attributed to the densely packed crystal lattice together with the narrow cavities around the axial ligands. In other words, the molecules have to be placed in a loosely packed crystal

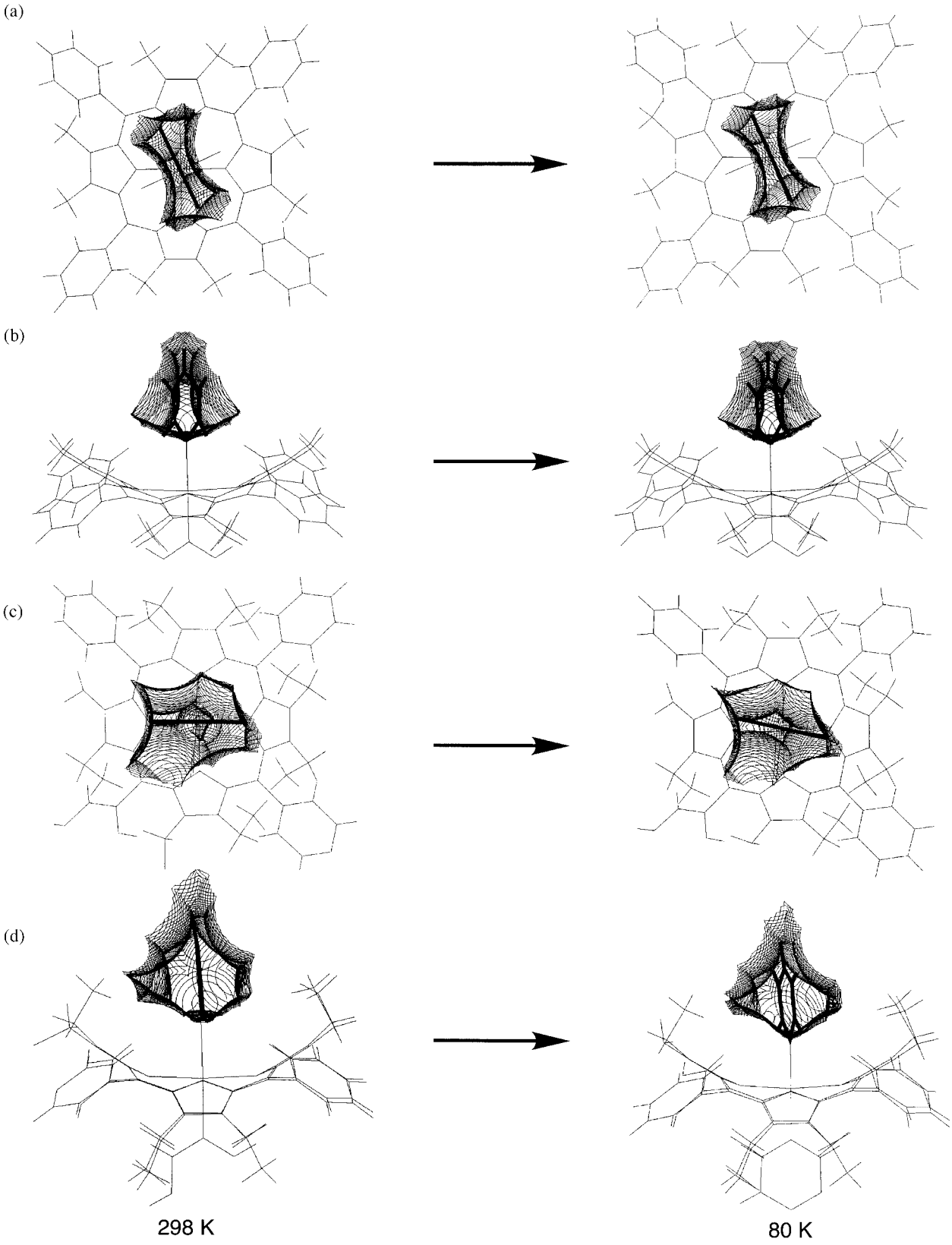

Figure 8. The orientation change of the pyridine ligands in the cavities of $[Fe(OMTPP)Py_2]ClO_4$ and $[Fe(OETPP)Py_2]ClO_4$ as the temperature is lowered from 298 K (left) to 80 K (right): (a) the cavity viewed along the normal to the average porphyrin plane of $[Fe(OMTPP)Py_2]ClO_4$, (b) the cavity viewed along the N2−N4 axis of $[Fe(OMTPP)Py_2]ClO_4$, (c) the cavity viewed along the normal to the average porphyrin plane of $[Fe(OETPP)Py_2]ClO_4$, and (d) the cavity viewed along the N1−N3 axis of $[Fe(OETPP)Py_2]ClO_4$

lattice and the cavities around the axial ligands have to be wide for the occurrence of the spin crossover in the solid state.

Experimental Section

General Procedures: Iron-57 Mössbauer spectra were measured on a Wissel Mössbauer spectrometer system consisting of an MDU-1200 function generator, a DFG-1200 driving unit and an MVT-100 velocity transducer, incorporating a model 7800 multi-channel analyzer form Seiko EG&G Co. Ltd. The samples were kept in a Heli-Tran LT-3 gas-flow cryostat from Advanced Research System Inc. equipped with a 9620 digital temperature controller from Scientific Instruments Inc. and the ^{57}Co(Rh) source was kept at room temperature. The data were analyzed using the standard least-squares method. The isomer shifts (δ) are given relative to α-iron foil at room temperature. The solid state magnetic susceptibilities were measured over the temperature range 2−300 K in a magnetic field of 0.5 T with a SQUID magnetometer (Quantum Design MPMS-7). The measured data were corrected for diamagnetic contributions.

Synthesis: H_2(OMTPP) and the iron(III) chloride complex [Fe(OMTPP)Cl] were prepared according to the literature.[45−49] [Fe(OMTPP)(THF)$_2$]ClO_4 was prepared by the addition of a THF solution of $AgClO_4$ to a THF solution of [Fe(OMTPP)Cl].[49,50] The bis-ligated complexes, [Fe(OMTPP)L_2]ClO_4, were prepared by the addition of 10−15 equiv. of the ligand (DMAP or Py) to a $CHCl_3$ solution of [Fe(OMTPP)(THF)$_2$]ClO_4.[49]

Crystal Structure of [Fe(OMTPP)(Py)$_2$]ClO_4·1/3$HClO_4$·4/3$CHCl_3$ at 298 K

i) Preparation of Crystals: The purple solid [Fe(OMTPP)(THF)$_2$]ClO_4 was dissolved in $CHCl_3$ containing 10−15 equiv. of pyridine and allowed to stand at room temperature. One of the cubic crystals thus obtained was sealed within a glass capillary to prevent evaporation of solvent in the crystal lattice.

ii) X-ray Crystal Structure Analysis: All data were collected on a Rigaku AFC-7R diffractometer with filtered Mo-K_α radiation (λ = 0.71069Å) and a rotating anode generator. Cell constants and an orientation matrix for data collection were obtained from a least-squares refinement using the setting angles of 21 carefully centered reflections in the range $30.08 < 2\theta < 33.66°$ corresponded to an *I*-centered cubic cell. The data were collected at room temperature using the ω scan technique to a maximum 2θ value of 54.9°. Of the 1948 reflections which were collected, 1681 were unique (R_{int} = 0.0362). An empirical absorption correction based on azimuthal scans of several reflections was applied which resulted in transmission factors ranging from 0.80 to 0.98.[51] The structures were solved by direct methods with the program SIR97,[52] TEXSAN[53] and expanded using the program DIRDIF94.[54] The structure refinement was carried out by the full-matrix least-squares method with SHELXL-97.[55] All non-hydrogen atoms were refined anisotropically. All the hydrogen atoms were located in calculated positions. The positional parameters of the H atoms were constrained to have C−H distances of 0.96Å for primary, 0.97Å for secondary, and 0.93 Å for aromatic H atoms. The H-atom *U* values were constrained to have 1.2 times the equivalent isotropic *U* value of the atoms to which they are attached (1.5 for methyl groups). The atomic scattering factors were taken from the International Tables for Crystallography.

CCDC-208539 to -208542 contain the supplementary crystallographic data for this paper. These data can be obtained free of charge at www.ccdc.cam.ac.uk/conts/retrieving.html [or from the Cambridge Crystallographic Data Centre, 12, Union Road, Cambridge CB2 1EZ, UK; Fax: (internat.) +44-1223/336-033; E-mail: deposit@ccdc.cam.ac.uk].

iii) Crystal Data, Experimental and Refinement Details for Crystal Structure Determination: Crystal data: $C_{62}H_{54}N_6O_4Cl$·0.33$HClO_4$·1.33$CHCl_3$; M_r = 1230.72 g mol^{-1}; crystal color: purple; crystal dimensions: 0.5 × 0.5 × 0.3 mm; cubic, *I*43*d* (#220); $a = b = c$ = 25.937(3) Å; α = β = γ = 90°; *V*= 17448(3)Å^3; *Z* = 12; ρ = 1.406 gcm^{-3}; R_{int} = 0.0362, R_σ = 0.060; $-18 < h < 33$, $0 < k < 23$, $-10 < l < 19$; Refinement: Refinement on F^2; $R[F^2 > 2s(F^2)]$ = 0.0423, *R*(all data) = 0.0889, wR^2 = 0.1042; *S* = 0.988; 1948 reflections; 0 restraints; 204 parameters; $w = 1/[\sigma^2(F_o^2) + (0.0625\ P)^2]$ where $P = (F_o^2 + 2F_c^2)/3$; $(\Delta/\sigma)_{max} < 0.001$; $\Delta\rho_{max}$ = 0.19 eÅ^3; $\Delta\rho_{min}$ = −0.249 eÅ^3

Crystal Structure of [Fe(OMTPP)(DMAP)$_2$]ClO_4·4$CHCl_3$

i) Preparation of Crystals: The purple solid [Fe(OMTPP)(THF)$_2$]ClO_4 was dissolved in $CHCl_3$ containing 10−15 equiv. of DMAP and allowed to stand at room temperature. One of the prismatic crystals thus obtained was sealed within a glass capillary to prevent evaporation of solvent in the crystal lattice.

ii) X-ray Crystal Structure Analysis: All measurements were carried out on a Rigaku RAXIS-RAPID Imaging Plate diffractometer with graphite monochromated Mo-K_α radiation (λ = 0.71069Å) and a rotating anode generator. Indexing was performed from 3 oscillations which were exposed for 7.5 minutes. The camera radius was 127.40 mm. Readout was performed in the 0.100 mm pixel mode. The data were collected at 80 K to a maximum 2θ value of 55.0°. A total of 110 images, corresponding to 222.0° oscillation angles were collected with 3 different goniometer settings. Exposure time was 2.70 minutes per degree. Data were processed with the PROCESS-AUTO program package. Of the 106877 reflections which were collected, 17126 were unique (R_{int} = 0.039). The linear absorption coefficient, μ, for Mo-K_α radiation is 6.9 cm^{-1}. A symmetry related absorption correction using the ABSCOR program was applied which resulted in transmission factors ranging from 0.869−0.933. The data were corrected for Lorentz and polarization effects.[55] The structure was solved by a procedure similar to that described above.

iii) Crystal Data, Experimental and Refinement Details for Crystal Structure Determination: Crystal data: $C_{70}H_{67}N_8O_4ClFe$. 4$CHCl_3$; M_r = 1602.02 g mol^{-1}; crystal color: purple; crystal dimensions: 0.2 × 0.1 × 0.1 mm; monoclinic, $P2_1/c$ (#14); *a*= 16.4556(5)Å, *b* = 23.7289(6)Å, *c* = 19.8424(6)Å; β = 91.924(1)°; *V* = 7743.6(4) Å^3; *Z* = 4; ρ = 1.374 gcm^{-3}; R_{int} = 0.0546, R_σ = 0.0278; $-19 < h < 21$, $-30 < k < 30$, $-25 < l < 25$; Refinement: Refinement on F^2; $R[F^2 > 2\sigma(F^2)]$ = 0.0899, *R*(all data) = 0.1205, wR^2 = 0.2543; *S* = 1.024; 17126 reflections; 0 restraints; 935 parameters; $w = 1/[\sigma^2(F_o^2) + (0.01785P)^2 + 2.5869P]$ where $P = (F_o^2 + 2F_c^2)/3$; $(\Delta/\sigma)_{max} < 0.001$; $\Delta\rho_{max}$ = 0.906 eÅ^3; $\Delta\rho_{min}$ = −0.725 eÅ^3

Crystal Structure of [Fe(OETPP)(DMAP)$_2$]ClO_4

i) Preparation of Crystals: The purple solid [Fe(OETPP)(THF)$_2$]ClO_4 was dissolved in $CHCl_3$ containing 10−15 equiv. of DMAP and allowed to stand at room temperature. One of the prismatic crystals thus obtained was sealed within a glass capillary to prevent evaporation of solvent in the crystal lattice.

ii) X-ray Crystal Structure Analysis: All measurements were carried out on a Rigaku RAXIS-RAPID Imaging Plate diffractometer with graphite monochromated Mo-K_α radiation (λ = 0.71069Å) and a rotating anode generator. Indexing was performed from 3 oscillations which were exposed for 1.5 minutes. The camera radius was 127.40 mm. Readout was performed in the 0.100 mm pixel mode. The data were collected at 298 K to a maximum 2θ value of 55.0°. A total of 110 images, corresponding to 386.5.0° oscillation angles were collected with 3 different goniometer settings. Exposure time was 1.70 minutes per degree. Data were processed using the PROCESS-AUTO program package. Of the 85871 reflections which were collected, 5022 were unique (R_{int} = 0.051). The linear absorption coefficient, μ, for Mo-K_α radiation is 5.1 cm^{-1}. A symmetry related absorption correction using the ABSCOR program was applied which resulted in transmission factors ranging from 0.885−0.975. The data were corrected for Lorentz and polarization effects.[56] The structure was solved by a procedure similar to that described above.

iii) Crystal Data, Experimental and Refinement Details for Crystal Structure Determination: Crystal data: $C_{74}H_{80}N_8ClFe$, M_r = 1172.76 g mol^{-1}; crystal color: purple; crystal dimensions: 0.5 × 0.4 × 0.1 mm; trigonal, $P3_121$(#152); $a = b$ = 22.595(9) Å, c = 13.967(5) Å; V = 6175(3) $Å^3$; Z = 3; ρ = 0.946 g cm^{-3}; R_{int} = 0.0615, R_σ = 0.0224; $-29 < h < 29$, $-29 < k < 29$, $-18 < l < 18$; Refinement: Refinement on F^2; $R[F^2 > 2\sigma(F^2)]$ = 0.0594, R(all data) = 0.0607, wR^2 = 0.1585; S = 1.087; 9164 reflections; 4 restraints; 413 parameters; $w = 1/[\sigma^2(F_o^2) + (0.1236\ P)^2 + 0.4276\ P]$ where $P = (F_o^2 + 2F_c^2)/3$; $(\Delta/\sigma)_{max} < 0.001$; $\Delta\rho_{max}$ = 0.991 $eÅ^3$; $\Delta\rho_{min}$ = −0.300 $eÅ^3$

Acknowledgments

We thank Professors Yuji Ohashi and Hidehiro Uekusa, Faculty of Science, Tokyo Institute of Technology for assistance with the X-ray measurements. This work was supported by the Grant in Aid (No. 14540521, M. N.) for Scientific Research from the Ministry of Education, Culture, Sports, Science and Technology, Japan. Thanks are due to the Research Center for Molecular-Scale Nanoscience, the Institute for Molecular Science (IMS).

[1] W. R. Scheidt, C. A. Reed, *Chem. Rev.* **1981**, *81*, 543−555.
[2] W. R. Scheidt, M. Gouterman, in *Iron Porphyrin, Part I* (Eds.: A. B. P. Lever, H. B. Gray), Addison-Wesley, Reading, MA, **1983**, pp. 89−139.
[3] W. R. Scheidt, in *The Porphyrin Handbook*, *Vol. 3* (Eds.: K. M. Kadish, K. M. Smith, R. Guilard), Academic Press, San Diego, **2000**, ch. 16, pp. 49−112.
[4] M. M. Maltempo, *J. Chem. Phys.* **1974**, *61*, 2540−2547.
[5] S. Fujii, T. Yoshimura, H. Kamada, K. Yamaguchi, S. Suzuki, S. Shidara, S. Takakuwa, *Biochim. Biophys. Acta* **1995**, *1251*, 161−169.
[6] H. Déméné, P. Tsan, P. Gans, D. Marion, *J. Phys. Chem. B.* **2000**, *104*, 2559−2569.
[7] Abbreviations: OMTPP or OETPP: dianions of 2,3,7,8,12,13,17,18-octamethyl- or 2,3,7,8,12,13,17,18-octaethyl-5,10,15,20-tetraphenylporphyrin. TMP, TPP, and T*i*PrP: dianions of 5,10,15,20-tetramesitylporphyrin, 5,10,15,20-tetraphenylporphyrin, and 5,10,15,20-tetraisopropylporphyrin. DMAP: 4-(dimethylamino)pyridine. Py: pyridine. 4-CNPy: 4-cyanopyridine dianion.
[8] A. Ikezaki, M. Nakamura, *Chem. Lett.* **2000**, 994−995.
[9] A. Ikezaki, M. Nakamura, *Inorg. Chem.* **2002**, *41*, 6225−6236.
[10] C. A. Reed, F. Guiset, *J. Am. Chem. Soc.* **1996**, *118*, 3281−3282.
[11] D. R. Evans, C. A. Reed, *J. Am. Chem. Soc.* **2000**, *122*, 4660−4667.
[12] T. Ikeue, T. Saitoh, T. Yamaguchi, Y. Ohgo, M. Nakamura, M. Takahashi, M. Takeda, *Chem. Commun.* **2000**, 1989−1990.
[13] J.-P. Simonato, J. Pecaut, L. Le Pape, J.-L. Oddou, C. Jeandey, M. Shang, W. R. Scheidt, J. Wojacynski, S. Wolowiec, L. Latos-Grazynski, J.-C. Marchon, *Inorg. Chem.* **2000**, *39*, 3978−3987.
[14] F. A. Walker in *The Porphyrin Handbook, Vol. 5* (Eds.: K. M. Kadish, K. M. Smith, R. Guilard), Academic Press, San Diego, **2000**, ch. 36, pp. 81−183.
[15] M. Nakamura, T. Ikeue, H. Fujii, T. Yoshimura, *J. Am. Chem. Soc.* **1997**, *119*, 6284−6291.
[16] M. Nakamura, T. Ikeue, H. Fujii, T. Yoshimura, K. Tajima, *Inorg. Chem.* **1998**, *37*, 2405−2414.
[17] T. Ikeue, Y. Ohgo, T. Saitoh, M. Nakamura, H. Fujii, M. Yokoyama, *J. Am. Chem. Soc.* **2000**, *122*, 4068−4076.
[18] S. Wolowiec, L. Latos-Grazynski, M. Mazzanti, J.-C. Marchon, *Inorg. Chem.* **1997**, *36*, 5761−5771.
[19] S. Wolowiec, L. Latos-Grazynski, D. Toronto, J.-C. Marchon, *Inorg. Chem.* **1998**, *37*, 724−732.
[20] M.-A. Pilard, M. Guillemot, L. Toupet, J. Jordanov, G. Simonneaux, *Inorg. Chem.* **1997**, *36*, 6307−6314.
[21] G. Simonneaux, V. Schünemann, C. Morice, L. Carel, L. Toupet, H. Winkler, A. X. Trautwein, F. A. Walker, *J. Am. Chem. Soc.* **2000**, *122*, 4366.
[22] Y. Ohgo, T. Saitoh, M. Nakamura, *Acta Crystallogr., Sect. C* **2001**, *57*, 233−234.
[23] Y. Ohgo, T. Saitoh, M. Nakamura, *Acta Crystallogr., Sect. C* **1999**, *55*, 1284−1286.
[24] M. Nakamura, T. Ikeue, Y. Ohgo, M. Takahashi, M. Takeda, *Chem. Commun.* **2002**, 1198−1199.
[25] K. M. Barkigia, M. W. Renner, J. Fajer, *J. Porhyrins and Phthalocyanins* **2000**, *5*, 415−418.
[26] T. Ikeue, Y. Ohgo, T. Yamaguchi, M. Takahashi, M. Takeda, M. Nakamura, *Angew. Chem. Int. Ed.* **2001**, *40*, 2617−2620.
[27] H. Ogura, L. Yatsunyk, C. J. Medforth, K. M. Smith, K. M. Barkigia, M. W. Renner, D. Melamed, F. A. Walker, *J. Am. Chem. Soc.* **2001**, *123*, 6564−6578.
[28] Y. Ohgo, T. Ikeue, M. Nakamura, *Inorg. Chem.* **2002**, *41*, 1698−1700.
[29] D. M. Collins, R. Countryman, J. L. Hoard, *J. Am. Chem. Soc.* **1972**, *94*, 2066−2072.
[30] D. Inniss, S. M. Soltis, C. E. Strouse, *J. Am. Chem. Soc.* **1988**, *110*, 5644−5650.
[31] M. K. Safo, G. P. Gupta, F. A. Walker, W. R. Scheidt, *J. Am. Chem. Soc.* **1991**, *113*, 5497−5510.
[32] W. R. Scheidt, J. L. Kirner, J. L. Hoard, C. A. Reed, *J. Am. Chem. Soc.* **1987**, *109*, 1963−1968.
[33] O. Q. Munro, H. M. Marques, P. G. Debrunner, K. Mohnrao, W. R. Scheidt, *J. Am. Chem. Soc.* **1995**, *117*, 935−954.
[34] Y. Ohgo, T. Ikeue, T. Saitoh, M. Nakamura, *Chem. Lett.* **2002**, 432−433.
[35] J. R. Sams, T. B. Tsin, in *The Porphyrins* (Ed.: D. Dolphin); Academic Press, New York, **1979**, vol. 4, ch. 9, pp 425−478.
[36] P. G. Debrunner, in *Iron Porphyrin Part III*, A (Eds. B. P. Lever, H. B. Gray), VCH, New York, **1989**, pp. 139−234.
[37] P. Gütlich, J. Ensling, in *Inorganic Electronic Structure and Spectroscopy*, *Vol. 1* (Eds.: E. I. Solomon, A. B. P. Lever), John Wiley & Sons, Inc., New York, **1999**, pp. 161−211.
[38] T. Ikeue, Y. Ohgo, M. Takahashi, M. Takeda, S. Neya, N. Funasaki, M. Nakamura, *Inorg. Chem.* **2001**, *40*, 3650−3652.
[39] H. Keutel, I. Käpplinger, E.-G. Jäger, M. Grodzicki, V. Schünemann, A. X. Trautwein, *Inorg. Chem.* **1999**, *38*, 2320−2327.
[40] W. R. Scheidt, D. K. Geiger, K. J. Haller, *J. Am. Chem. Soc.* **1982**, *104*, 495−499.
[41] M. K. Ellison, H. Nasri, Y.-M. Xia, J.-C. Marchon, C. E. Schulz, P. G. Debrunner, W. R. Scheidt, *Inorg. Chem.* **1997**, *36*, 4804−4811.

[42] Y. Ohashi, K. Yanagi, T. Kurihara, Y. Sasada, Y. Ohgo, *J. Am. Chem. Soc.* **1981**, *103*, 5805−5812.
[43] A. Uchida, Y. Ohashi, Y. Sasada, *Nature (London)* **1986**, *320*, 51−52.
[44] A. Bondi, *J. Phys. Chem.* **1964**, *68*, 441−451.
[45] K. M. Barkigia, M. D. Berber, J. Fajer, C. J. Medforth, M. W. Renner, K. M. Smith, *J. Am. Chem. Soc.* **1990**, *112*, 8851−8857.
[46] L. D. Sparks, C. J. Medforth, M.-S. Park, J. R. Chamberlain, M. R. Ondrias, M. O. Senge, K. M. Smith, J. A. Shelnutt, *J. Am. Chem. Soc.* **1993**, *115*, 581−592.
[47] R.-J. Cheng, P.-Y. Chen, P.-R. Gau, C.-C. Chen, S.-M. Peng, *J. Am. Chem. Soc.* **1997**, *119*, 2563−2569.
[48] M. Nakamura, T. Yamaguchi, Y. Ohgo, *Inorg. Chem.* **1999**, *38*, 3126−3131.
[49] T. Ikeue, Y. Ohgo, T. Saitoh, T. Yamaguchi, M. Nakamura, *Inorg. Chem.* **2001**, *40*, 3423−3434.
[50] H. Ogoshi, H. Sugimoto, E. Watanabe, Z. Yoshida, Y. Maeda, H. Sakai, *Bull. Chem. Soc. Jpn.* **1981**, *54*, 3414−3419.
[51] A. C. T. North, D. C. Phillips, F. S. Mathews, *Acta Crystallogr., Sect. A* **1968**, *24*, 351−359.
[52] A. Altomare, M. C. Burla, M. Camalli, G. L. Cascarano, C. Giacovazzo, A. Guagliardi, A. G. G. Moliterni, G. Polidori, R. Spagna, *J. Appl. Cryst.* **1999**, *32*, 115−119.
[53] TEXSAN, *Crystal Structure Analysis Package, MSC/AFC Diffractometer Control Software*, Molecular Structure Corporation Houston; MSC, 3200 Research Forest Drive, The Woodlands, Texas 77381, USA, **1992**
[54] The DIRDIFß94 Program System, P. T. Beurskens, G. Admiraal, G. Beurskens, W. P. Bosman, R. de Gelder, R. Israel, J. M. M. Smits, Technical Report of the Crystallography Laboratory, University of Nijmegen, The Netherlands, **1994**.
[55] G. M. Sheldrick, SHELXL-97, *Program for the Refinement of Crystal Structures*, University of Göttingen, Germany, **1997**.
[56] T. Higashi, Program for Absorption Correction, Rigaku Corporation, Tokyo, Japan.

Received August 13, 2003
Early View Article
Published Online January 14, 2004

